Optical and Quantum Electronics (2023) 55:953
https://doi.org/10.1007/s11082-023-05173-1

Centrosymmetric structure of novel barium (II)-dibenzo-15-crown-5-ether-zinc (II)-tetra-thiocyanate single crystal for nonlinear optical application

V. Ravisankar[1] · V. Ramesh[1] · B. Gunasekaran[1] · Suresh Perumal[2] · P. Karuppasasmy[3] · T. Kamalesh[4]

Received: 30 May 2023 / Accepted: 10 July 2023 / Published online: 28 August 2023

Abstract
A novel barium (II)-dibenzo-15-crown-5-ether-zinc (II)-tetra-thiocyanate single crystal were synthesized by using slow evaporation method at ambient temperature. Crystallography structural information such as lattice parameters, symmetry and reliability factor were confirmed by single-crystal X-ray diffraction pattern. Additionally, crystalline planes were investigated by powder XRD studies. It reveals monoclinic structure with the centrosymmetric space group of $P2_{1/n}$. The as prepared material functional groups of CN stretching of SCN, metal-nitrogen bonding and Ba–O group well-identified. The optical cut-off wavelength was found to be 276 nm and the band gap value is 4.1 eV. Moreover, the correlation of exterior topography, reverse growth rate and synthesized elements were confirmed by FE-SEM, chemical etching, EDS and CHNS analysis. TG–DTA and Vickers hardness studies revealed the material stability and strength. Additionally, the third-order nonlinear optical properties examined by Z-scan technique using wavelength of 633 nm. The nonlinear refractive index (n_2) = 2.33×10^{-9} cm^2 W^{-1}, absorption coefficient (β) = 0.20×10^{-3} cm W^{-1} and third-order susceptibility (χ^3) = 1.49×10^{-5} esu, were experimentally calculated.

Keywords Single crystal XRD · UV–Visible-NIR · FTIR · Etching · Thermal analysis · Z-scan studies

1 Introduction

Over the last two decades, the search for novel organometallic non-linear optical (NLO) frequency conversion materials used in numerous laser and optical device applications. Hence, to grow organometallic NLO crystals formed in a series of inorganic polymers with organic spacers (IPOS) complexes. To enhance NLO characteristics, organic and inorganic components are combined to create organometallic thiocyanate compounds. This category of material exhibits centrosymmetric crystal structures and fast optical response. Additionally, the physiochemical properties of the IPOS series have moderate thermal, mechanical strength and a high surface laser damage threshold (Ramesh et al. 2020; Kumar et al. 2016; Sakthi et al. 2016). Organometallic thiocyanate NLO-based crystalline materials play a

Extended author information available on the last page of the article

crucial role in the emerging fields of optical switching, data storage, information processing, optical communications and laser technology (Pabitha and Dhanasekaran 2012, 2013; Bhushan Kumar et al. 2015; Saravanan et al. 2018).

The IPOS series of bimetallic thiocyanate complex types is AB $(SCN)_4$, where A is alkali earth metals (Ba^{2+}, Mg^{2+}, Cd^{2+}), B is transition metals (Zn^{2+}, Mn^{2+}, Co^{2+}) and ligands (thiocyanate, thiourea) (Ramesh and Rajarajan 2013; Rajarajan and Sendil Kumar 2013; Ramesh et al. 2019, 2019). The structural formation of organometallic compounds forms a two or three-dimensional bridging network. According to double ligand theory, the IPOS series points out unique intramolecular charge transfers from ligand to metal, metal to ligand, or d-d transitions. In addition, the presence of delocalized π electrons is well-suited for large molecular hyper polarizability. The versatile thiocyanate ligand (SCN^-) with two donor atoms, S and N, binds with metal ions to form a molecular crystal structure. Based on the concept of hard-soft-acid–base, these types of structural modifications depend on the accepters, like soft S-atoms and hard N-atoms, which always bind to the ligand (Usha et al. 2015; Gunasekaran and Ponnusamy 2006; Balarew and Duhlew 1984; Showrilu et al. 2020). The major factors, such as transition metals, ligands, cavity size and coordination numbers, are potentially used to construct the organometallic thiocyanate complex. The physicochemical properties of BCMTC, BCCTC and BDBCCTC (Ravisankar et al. 2021a, 2022, 2021b) crystals are reported in our research group.

In the present investigation, we designed the chemical structure of Ba^{2+} ions bonded to benzo 15-crown-5 ether and the Zn^{2+} ions bonded to -S-C≡N- ligand forming two or three-dimensional bridging networks. A new series of barium (II)-benzo 15-crown-5-ether zinc (II)-tetra-thiocyanate (BDBCZTC) single crystal synthesized by using the slow evaporation technique. Single crystal and powder X-ray diffraction (SXRD and PXRD) studies reveal grown crystal structural information. The title structure refinement was deposited in the Cambridge Crystallographic Data Center (CCDC No: 2107693). The spectroscopic studies such as Fourier transform infrared (FT-IR), UV–Visible-NIR, energy dispersive X-ray spectrum (EDS) and CHNS was measured systematically. The thermal and mechanical properties of the prepared crystal were examined by TG/DTA and Vickers hardness studies. The sample morphology, reverse growth rate were visualized by FE-SEM and chemical etching analysis. Furthermore, using the Z-scan technique the third order nonlinear optical (TONLO) properties are deliver the saturable absorption (SA) and self-defocusing (SDF) nature.

2 Experimental procedure

2.1 Material synthesis and crystal growth

Barium (II)-dibenzo-15-crown-5-ether-zinc (II)-tetra-thiocyanate single crystal were synthesized by using slow evaporation method. The chemical scheme and reaction equation are as follows (Fig. 1a):

$$BaCl_2 + ZnCl_2 + 2\left(C_{14}H_{20}O_5\right) + 4\left(NH_4SCN\right) \rightarrow \left[Ba\left(C_{14}H_{20}O_5\right)_2 \cdot Zn\left(SCN\right)_4\right] + 4NH_4Cl$$

All the precursor materials were purchased in AR grade. Initially, an appropriate amount of $BaCl_2$, $ZnCl_2$ and NH_4 (SCN) were taken in the ratio of 1:1:4 and stirred for 1 h. Simultaneously, the benzo-15-crown-5-ether solution was stirred for 1 h, then added slowly

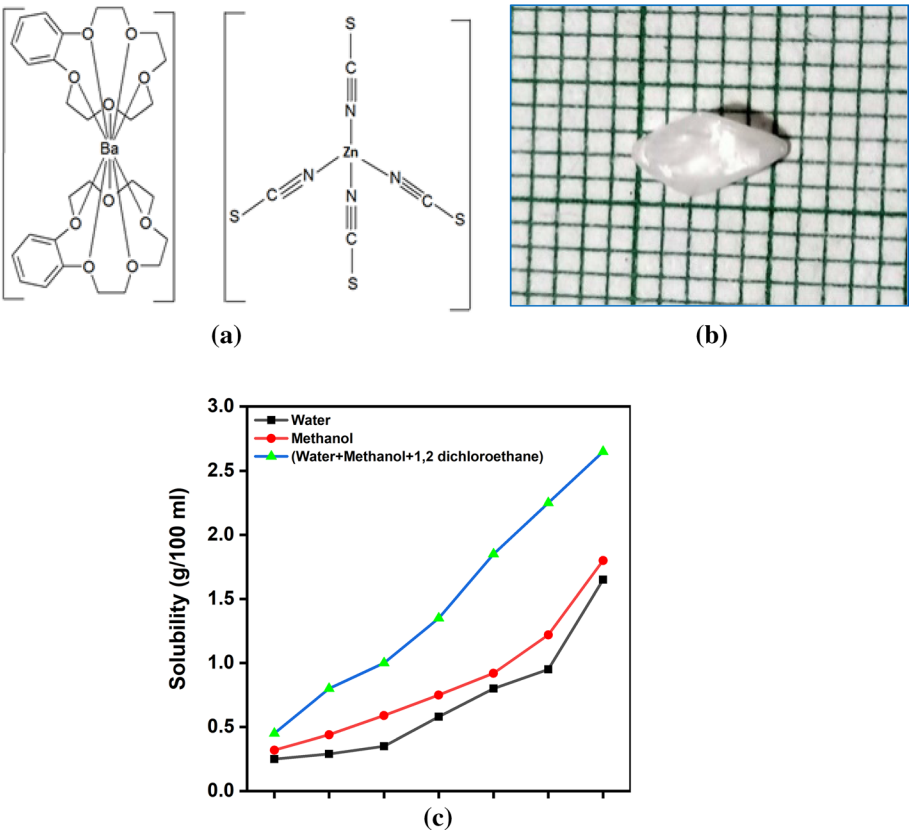

Fig. 1 **a** Chemical scheme and 1 **b** Photograph of BDBCZTC single Crystal. **c** Solubility curve of BDBCZTC

dropwise manner in to the three mixture solutions. The resultant product was stirred continuously for 8 h. Finally, a small amount of precipitate settled at the bottom of the beaker. To avoid co-precipitation the reaction product was gently heated above room temperature (to a maximum + 5 °C) to increase the solubility of the solution. The resultant homogenous solution was filtered with whatman paper and kept for crystallization. The grown crystal size $6 \times 4 \times 2$ mm^3 were harvested after 20–25 days. The snap of full-fledged BDBCZTC single crystal is shown in Fig. 1b.

2.2 Solubility studies

The solubility as a function of temperature (30-60℃) of the grown crystal were measured in different solvents. For this study using various kinds of solvents for instance water, methanol and 1–2 dichloroethane taken in the ratio of 2:2:1 and optimized after various trials. Here the observed solubility graph explicitly showed that solubility of the solute is directly proportional to temperature. Hence, the title compound was very less soluble in water, and moderately soluble in methanol. Figure 1c depicts the solubility of BDBCZTC solvent versus different temperature.

3 Result and discussions

3.1 Structure determination: single crystal and powder X-ray diffraction

The title compound crystallographic data were collected from SXRD analysis. The direct method procedure used to solve the title compound, as implemented in SHELXS97 and refined by SHELXL2018 (Bruker AXS 2008; Sheldrick 1996, 2008). The positions of non H-atoms are identified using the full-matrix least-square method (Ravisankar et al. 2021c). It reveals a monoclinic with space-group (centrosymmetric) $P2_1/n$ and detailed structural information interpreted in Table 1 (CCDC: 2,107,693). Figure 2a, the title compound molecule 30% probability ellipsoid ORTEP scheme is depicted, final reliability (R) factor is 0.0550. Here, central atoms Ba^{II} and Zn^{II} ions are located at the center of two-fold rotational axes. Half of the asymmetric arrangements consisted of anion and cation atoms. In this structure, Zn^{II} ion surrounded by four SCN, Ba^{II} ion strongly bonded with 10 oxygen atoms from two benzo-15-crown-5 ether in a sandwich-like configuration. The bond lengths Ba–O and Zn–N are well matched with related complex structures. The molecular packing of the grown crystal stabilized by weak C–H…S intermolecular H-bond is depicted in Fig. 2b. The H-bond data information is given in Table 2. Additionally, to analyse the crystalline formation and then lattice parameters are verified in PXRD studies. Vesta software was used to index all the diffraction planes as shown in Fig. 3. An intense sharp peak (111) at 10.79° confirms the crystalline nature of the title compound. The PXRD data (hkl) are listed in Table 3 and observed cell parameters: $a = 12.067(2)$ (Å), $b = 20.112(3)$ (Å), $c = 17.408(4)$ (Å), $\alpha = \gamma = 90°$, $\beta = 101.046(5)°$ and $V = 4146.3(13)$ $Å^3$ well agreed upon the SXRD data.

Table 1 Crystal data, data collection and structure refinement

Identification code	SHELX
Chemical formula	$C_{32}\ H_{40}\ Ba\ O_{10}\ N_4\ S_4\ Zn$
Formula weight	971.64
Crystal system, space-group	Monoclinic, $P2_1/n$
Cell dimensions	a = 12.067(2) Å, b = 20.112(3) Å, c = 17.408(4) Å: $\alpha = \gamma = 90°$, $\beta = 101.046(5)$
T (K)	296
λ (Å)	0.71073
V ($Å^3$)	4146.3(13)
D_x (g/cm^3)	1.556
Z	4
hkl ranges	$-18 \le h \le 18, -15 \le k \le 15, -21 \le l \le 21$
Θ range (°)	1.56–26.61
No. of parameters	469
Goodness of fit	1.052
R (F) [$I > 2\sigma$ (I)]	0.0390
R (F) (all data)	0.0700
wR(F^2) [all data]	0.1056
Max/min Δρ ($e.Å^{-3}$)	0.618/−0.538

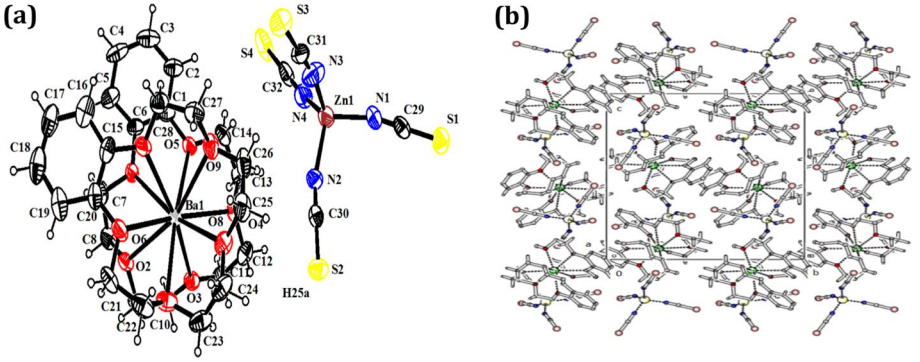

Fig. 2 **a** ORTEP plot of the compound drawn at 30% probability ellipsoid level. **b** crystal packing of the title compound, viewed along the 'b' axis. H-bonds are shown as dashed lines

Table 2 Hydrogen bond data and angle (Å and °) of the compound

D-H…A	D-H	H…A	D…A	DHA
C11-H11A…S1	0.97	3.02	3.921(8)	154.5
C14-H14B…S4	0.97	3.00	3.831(7)	144.8
C21-H21B…S1	0.97	2.95	3.760(8)	141.3
C10-H10A…S2	0.97	2.97	3.596(7)	123.8
C26-H26B…N2	0.97	2.64	3.519(11)	150.3

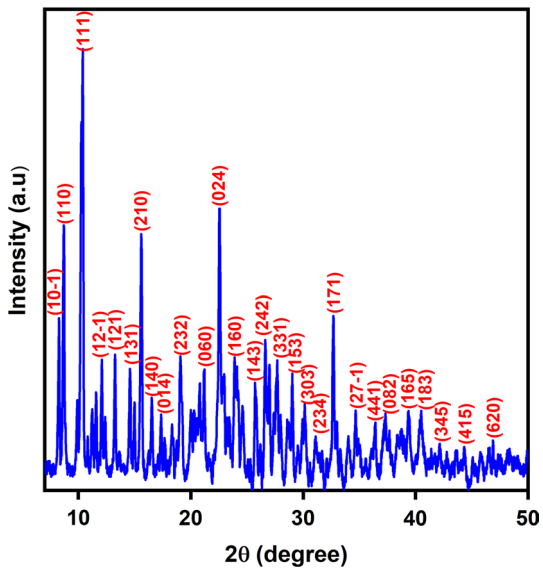

Fig. 3 PXRD profile of BDB-CZTC

Table 3 Selected PXRD spectral data of BDBCZTC

Peak no	h k l	d (Å)	F (real)	|F|	2θ	Intensity
1	1 0 -1	10.7445	214.601	20.061	8.24234	25.081
2	1 1 0	10.2047	213.668	18.6835	8.67916	44.7696
3	1 1 1	8.18616	78.2981	6.03121	10.7988	7.72551
4	1 2 -1	7.34181	170.469	15.9192	12.045	29.4417
5	1 2 1	6.69052	− 177.76	− 19.659	13.2547	13.2298
6	2 1 -1	5.71362	155.314	33.3767	15.4962	15.1882
7	2 1 0	5.68015	168.018	14.0921	15.626	8.41009
8	1 3 1	5.36811	122.051	24.4949	16.5003	8.20285
9	1 4 0	4.62794	115.951	24.3386	19.1624	5.46456
10	0 1 4	4.17818	75.7015	6.02209	21.2479	1.81295
11	0 2 4	3.93139	199.356	20.3617	22.6542	5.52396
12	2 3 2	3.72543	244.167	− 24.956	23.8659	14.8626
13	1 4 3	3.46682	− 216.97	− 5.01	25.6755	9.96677
14	0 6 0	3.35183	− 466.15	− 31.988	26.5722	21.4827
15	2 4 2	3.34526	− 115.78	− 0.473	26.6911	1.30663
16	3 3 1	3.23536	− 190.2	− 27.736	27.6154	3.35031
17	1 5 3	3.0794	− 65.35	− 13.995	29.0439	0.3638
18	3 0 3	2.98741	79.9247	8.61935	29.9589	0.24629
19	2 3 4	2.87794	187.528	26.461	31.0496	5.0637
20	1 7 1	2.73586	61.5913	4.96504	32.7875	0.23962

Symmetry operators: (i) x, y, z (ii) –x + 1/2, y + 1/2, -z + 1/2 (iii) -x, -y, -z (iv) x-1/2, -y-1/2, z-1/2.

3.2 UV–Visible-NIR studies

The grown crystal UV cut-off wavelength was found to be 276 nm as shown in Fig. 4a and b which is comparable to other thiocyanate complex materials (ZCTC-248 nm, CMTG-290 nm and LATC-320 nm) nearly same (Cynthia et al. 2017; Vetha Potheher et al. 2013; Suresh et al. 2018). Furthermore, the sample exhibits broad optical transparency across the entire visible and NIR region up to 2000 nm. Hence, it is decided that a very high

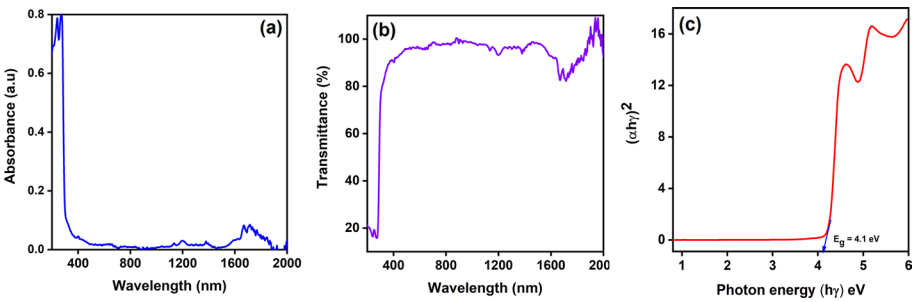

Fig. 4 **a** UV–Vis-NIR Absorption, **b** Transmission spectrum, **c** Bandgap (Tauc's plot)

transmittance percentage exists. It clearly shows that the title crystal is suitable for NLO and photonic applications. The band gap (E_g) can be estimated using Tauc's relation.

$$E_g = \frac{1240}{\lambda} eV \tag{1}$$

$$\alpha h\gamma = A\left(h\gamma - E_g\right)^2 \tag{2}$$

where 'h' is Planck's constant (6.626×10^{-34} J/s) and 'E_g' bandgap was estimated (Tauc's plot) at 4.1 eV shown in Fig. 4c. The theoretical bandgap calculated value of 4.3 eV is quite similar to the measured experimental values. The above results show a larger bandgap value can have superior optical conductivity (Penn 1962).

3.3 Vibrational spectroscopy studies

The presence of various absorption frequencies (400 to 4000 cm^{-1}) of the title compounds NH_4 (SCN) and $C_{14}H_{20}O_5$ carried out in the ATR mode is shown in Fig. 5a. The absorption peaks of 2928 and 2880 cm^{-1} were observed at C–H stretching vibrations (Ravisankar et al. 2021a). The CN or CS stretching vibration mode of NH_4 (SCN) gets shifted to 2054 cm^{-1}. The Ba^{2+}, Zn^{2+} are hard and soft electron acceptors, whereas N (SCN) and S (SCN) are donors connected by a thiocyanate ligand (Ravisankar et al. 2022). The CN and CS bond was assigned in 1407 cm^{-1}. The two peaks 1357 and 1300 cm^{-1} are assigned to C–H rocking vibration and C–H wagging, respectively. The C–O stretching vibration occurs at 1247 cm^{-1} and =C–H bending vibration spectra sited in 948 cm^{-1} (Ravisankar et al. 2021a). The metal-nitrogen strength were observed at 524 cm^{-1}. The SCN bending vibration (N bonding) were identified at 479 cm^{-1} (Cynthia sundararaj, Suresh sagadevan 2018). Figure 5b micro-Raman spectra reveal sharp intensity peak at 2059 cm^{-1} indicating the SCN ligand presented in BDBCZTC single crystal. Moreover, CS stretching vibrational modes are observed at 764 cm^{-1}. The SCN bonding vibration (N bonding) presented at 741 cm^{-1}. Finally, the existence of BaO group were observed in lower wavelengths 276, 138 and 105 cm^{-1} respectively. The comparative spectral assignments are given in Table 4.

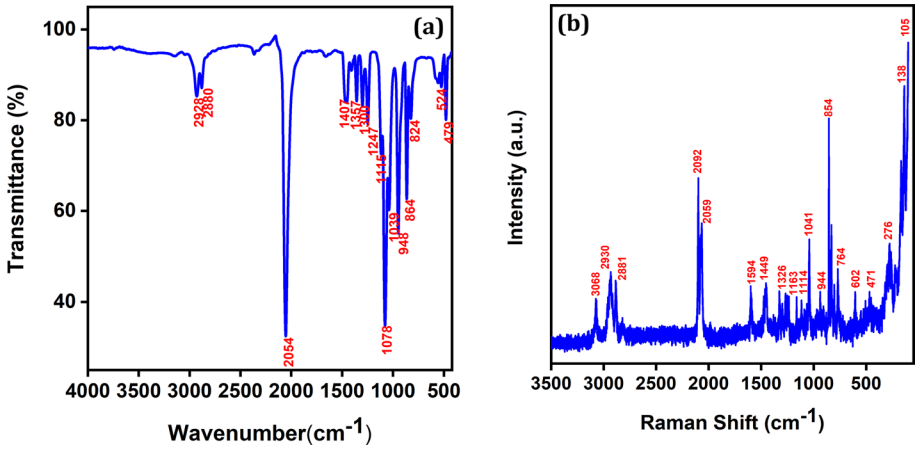

Fig. 5 **a** FT-IR, **b** Micro-Raman spectrum of BDBCZTC

Table 4 FT-IR and micro-Raman spectral assignments of BDBCZTC

Wave number (cm^{-1})		Band assignments
IR	Raman	
2928–2880	2930–2881	C–H stretching vibration
2054	2059	CN-stretching vibration of SCN (thiocyanate)
1407	1449	Symmetric stretching of CN and CS bond
1357	–	C–H rock vibration
1247	–	C–O stretching vibration
948	944	=C–H bending vibration
524	–	Metal-Nitrogen stretch
479	471	SCN bending vibration (N bonding)

3.4 FE-SEM and EDS mapping

The exterior topography of grown crystal investigated by FE-SEM technique. The growth pattern can be scanned at different magnifications (4, 5 µm and 500 nm) as shown in Fig. 6(a, b and c). The micrograph clearly reveals the well-ordered small micro-crystal-like morphological patterns are evident which show the perfect growth of the crystal from the 2D nucleation mechanism. Hence, the observed SEM micrographs confirm that grown crystals have good crystalline nature. Therefore, defect less crystals are employed to make devices. Additionally, the EDS spectrum in Fig. 7 shows the presence of barium (Ba), zinc (Zn) and thiocyanate ligand (SCN). The experimentally observed and expected (theoretically calculated values) chemical composition are given in Table 5.

3.5 CHNS analysis

CHNS analysis accurately identifies the carbon, hydrogen, nitrogen and sulphur composition percentages. A percentage of the elements in the formula (C_{32} H_{40} Ba Zn N_4 O_{10} S_4) are used to analyze these experimental results. The examined sample can be decided as the expected compound if the deviation of elemental analysis results from the calculated is less than 0.9%. The atomic weight % of theoretical and experimental S, C, H and N are summarized in Table 6. Hence, it confirms the presence of compounds of BDBCZTC.

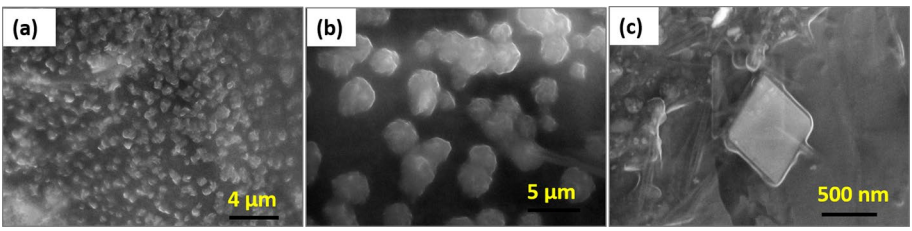

Fig. 6 (**a**, **b** and **c**) FE-SEM micrograph images for BDBCZTC single crystal

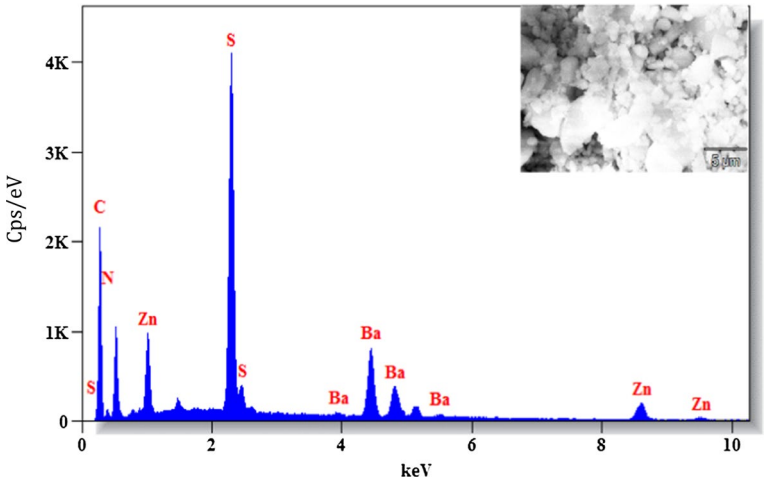

Fig. 7 EDS spectrum for BDBCZTC

Table 5 Elemental composition of BDBCZTC

Elements	Mass [%]	Atom [%]
C	31.60	67.30
S	15.48	14.88
Ba	21.54	3.941
Zn	7.366	10.44
N	5.535	3.43
Total	81.52	100

Table 6 CHNS data of BDBCZTC

Elements	Chemical compositions (%)	
	Theoretical	Experimental
N	5.77	6.965
C	39.55	38.356
H	4.15	3.003
S	13.20	14.989

3.6 Chemical etching studies

Etching analysis assures the growth mechanism. Typically, NLO applications require defect-free single crystals. The title compound etchant patterns were examined under an optical microscope. In this process etching concentration ratio and time play major roles. The solvents are water, ethanol and methanol (2:2:1) used as an etchant. Figure 8a shows without the etching surface, after the etching time (10 to 30 s) the hill rock step pattern growth was observed in the crystal surface as shown in Fig. 8(b and c). The calculated etch pit density (EPD) formula.

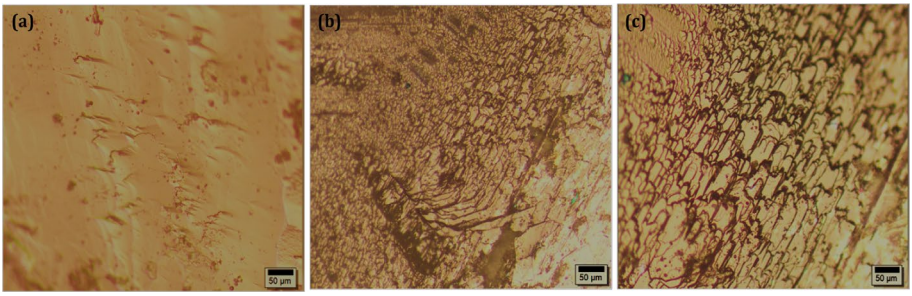

Fig. 8 **a** Before etching, **b** After Etching 10 s, and **c** After etching 30 s for BDBCZTC

$$\text{Etch pit density} = (\text{Number of etch pits}) / (\text{Area}) \tag{3}$$

The estimated EPD value was 3×10^3 cm^{-2}. The value of BDBCZTC is much better when compared to organometallic thiocyanate CMTC single crystal (103 cm^{-2}) (Hegde 2018). Therefore, the internal structural symmetry of the grown crystals reveals a 2D growth mechanism.

3.7 Mechanical strength measurement

The mechanical properties influenced by hardness number (H_V), yield strength (σ_y), brittleness and stiffness constant (C_{11}) is related to crystal structure and bond strength. However, any practical device construction can be done using the mechanical strength test. The diamond pyramidal indentation impression was made on the polished crystal surface and the varying applied loads (P) from 10 to 100 g and diagonal indented impression (d) were observed by microscope. A few cracks appeared at 100 g load on the crystal surface. The formula for H_V is

$$H_v = 1.854 \frac{P}{d^2} \left(\frac{\text{Kg}}{\text{mm}^2} \right) \tag{4}$$

Figure 9a shows that various Hv with applied loads (P) means hardness increases as load increases. Mayer's index number (n) is plotted for logarithm (P) and logarithm (d) shown in Fig. 9b. Using, the straight-line slope method yields with n were calculated to be 1.19, concluding the grown crystal hard category. Other properties such as $\sigma_y = (H_v^{7/3})$ and $C_{11} = H_v/3$ proportional to the P are displayed in Fig. 9c and d. An estimated value is tabulated in Table 7. BDBCZTC crystal deliver better stability compared to other thiocyanate family MCCTC, MMTC and BDBCCTC (Ravisankar et al. 2021a; Joseph et al. 2006; Sun 2005).

3.8 Thermal analysis

The grown crystal decomposition and thermal stability were examined by using TG–DTA analysis. The temperature of the sample was stabilized up to 139 °C and sustained without weight loss from 34 to 100 °C, as shown in Fig. 10. Following significant

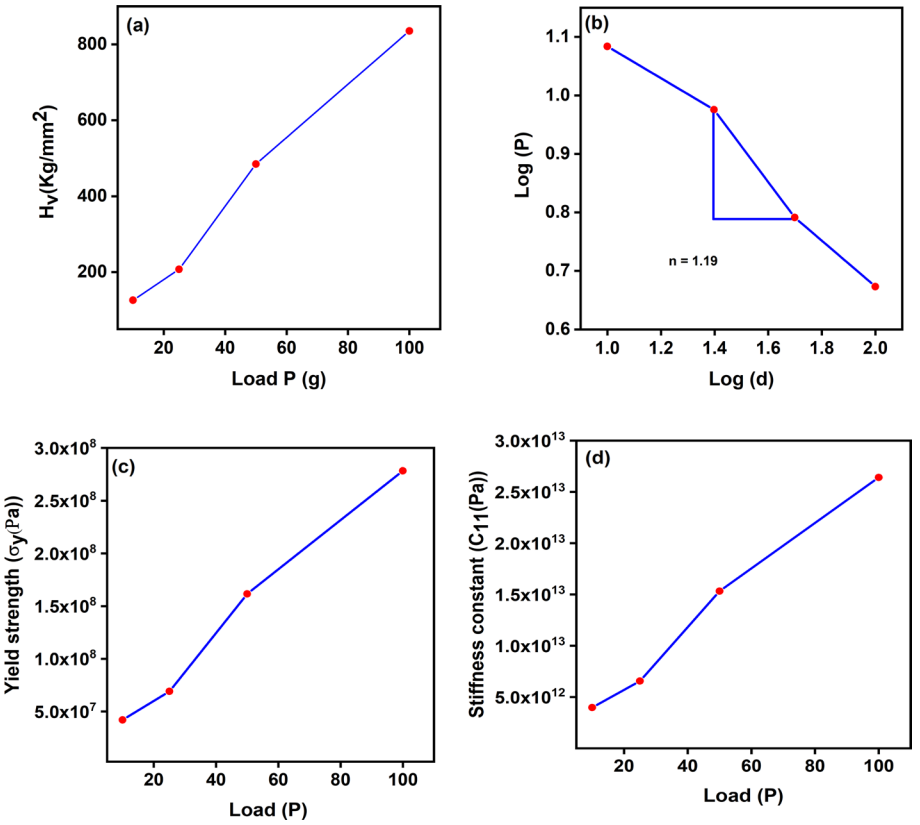

Fig. 9 **a** Vickers Hardness (Hv) vs. Load (P) **b** Logarithm (P) vs. Logarithm (d) **c** Yield strength (σ_y) vs. Load (P) **d** Stiffness Constant (C_{11}) vs. Load (P)

Table 7 Vickers hardness values of BDBCZTC single-crystal

S. no	Load (P) g	Vickers hardness (Hv) Kg/mm^3	Yield Strength ($\sigma_y = (H_v^{7/3})$) Pa	Stiffness constant $C_{11} = (Hv^{7/4})$ Pa
1	10	126.067	4.20×10^7	3.99×10^{12}
2	25	207.389	6.91×10^7	6.56×10^{12}
3	50	484.495	16.1×10^7	1.53×10^{13}
4	100	835.024	27.8×10^7	2.64×10^{13}

weight loss to confirm the decomposition of the sample, The DTA curve shows a sharp breakdown has happened at the 334 °C strong endothermic peak observed, and it confirming the obvious decomposition temperature of prepared material. The stability value of title compound was comparatively far better than that of other thiocyanate crystals such as CMTC (251 °C), MCCTC (171 °C), and CMTD (150 °C) (Hegde 2018; Sun 2005; Cynthia and Milton Boaz 2013).

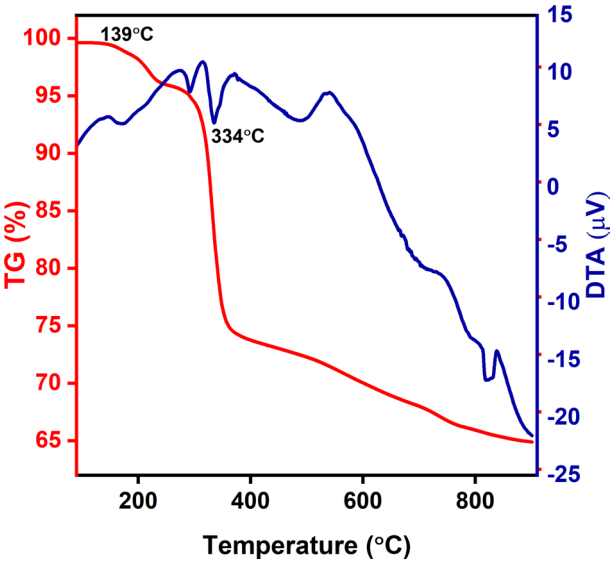

Fig. 10 TG–DTA profile of BDBCZTC

3.9 Dielectric studies

The dielectric properties of materials provide information about the electrical distribution within the material and are widely applicable for optoelectronic applications. At room temperature (303 K), the sample was tested at frequencies ranging from 3 to 5 MHz. The estimated dielectric constant (ε_r) relation

$$\varepsilon_r = \frac{Cpd}{\varepsilon_0 A} \tag{5}$$

Figure 11a shows the dielectric constant (ε_r) and log frequency at room temperature. It is concluded that higher ε_r in the lower frequency region except for space charge polarization which reveals perfect crystalline form. Figure 11b shows the dielectric loss (tan δ) and

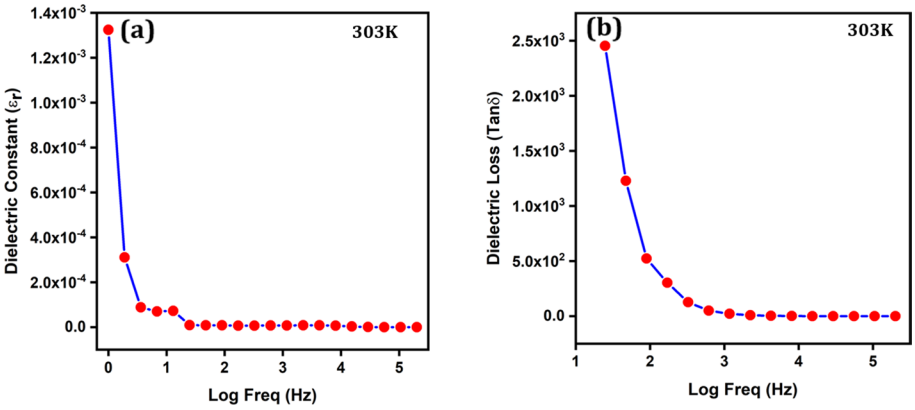

Fig. 11 **a** Dielectric constant (ε_r) **b** Dielectric loss (tanδ) of vs. Logarithm Frequency (Hz)

log frequency at room temperature, exhibiting the low value of tan δ at low frequencies showing that grown crystal (BDBCZTC) has fewer defects.

3.9.1 Dielectric solid-state parameters (SSP)

SSP factors of a valence electron, plasma energy ($\hbar\omega_P$), Penn gap (E_P), Fermi energy (E_F) can be calculated theoretically. The estimated values are utilized in electronic polarizability (α) and dielectric susceptibility. M = 971.64 g/mol is the molecular weight ($C_{14}H_{20}O_5$), unit cell (Z = 4), $N_A = 6.023 \times 10^{23}$ mol^{-1} (Avogadro's number) and volume (V) is the 4146.3(13) Å. The calculated density (ρ) is 1.556 g/cm^3. The plasma energy ($\hbar\omega_P$) (Jackson 1978)

$$\hbar\omega_P = 28.8\left(\frac{Z' \times \rho}{M}\right)^{\frac{1}{2}} \tag{6}$$

The total number of valance electrons in the compound is given in the title as Z' = [(28 × Z'$_C$) + (40 × Z'$_H$) + (1 × Z'$_{Ba}$) + (1 × Z'$_{zn}$) + (4 × Z'$_N$) + (10 × Z'$_O$) + (4 × Z'$_S$) = 260. Here is the valence electron substitution for each of C(4), H(1), Ba(2), Zn(2), N(5), O(6), and S(6). ε_r at 1 Hz for room temperature. Penn model, E_P and E_F are given by Penn (1962); Ravindra and Srivastava 1980)

$$E_p = \frac{\hbar\omega_P}{(\varepsilon' - 1)^{\frac{1}{2}}} \tag{7}$$

$$E_F = 0.2948\left(\hbar\omega_P\right)^{\frac{4}{3}} \tag{8}$$

Additionally, electronic polarizability (α) was calculated using the relation

$$\alpha = \left[\frac{\left(\hbar\omega_P\right)^2 S_0}{\left(\hbar\omega_P\right)^2 S_0 + 3E_p^2}\right] \times \frac{M}{\rho} \times 0.396 \times 10^{-24}\text{cm}^3 \tag{9}$$

where S_o is constant, then the electronic polarizability (α) depends on Clausius Mossotti (CM) relation, band gap (E_g) and coupled dipole method (CDM) using the following relations (Nijboer and Renne 1968)

$$\alpha = \frac{3M}{4\pi N_A \rho}\left(\frac{\varepsilon' - 1}{\varepsilon' + 2}\right) \tag{10}$$

$$\alpha = \left[1 - \frac{\sqrt{Eg}}{4.06}\right]\left[\frac{M}{\rho}\right] 0.396 \times 10^{-24}\text{cm}^3 \tag{11}$$

$$\alpha = \frac{Z'e^2}{m_o \omega_o^2} \tag{12}$$

The estimated electrical properties (Penn analysis and CM relation) of BDBCZTC are shown in Table 8.

Table 8 Solid-State parameter of BDBCZTC single-crystal

SSP-factors	Calculated values of BDBCZTC crystal
Plasma energy ($\hbar\omega_p$) eV	18.585
Penn gap energy (E_P) eV	0.287
Fermi energy (E_F) eV	13.165
Electronic polarizability (α) using Penn analysis (cm^3)	2.456×10^{-22}
Electronic polarizability (α) with CM relation (cm^3)	2.427×10^{-22}
Electronic polarizability (α) with E_g (cm^3)	1.228×10^{-22}
Electronic polarizability (α) with CDM (cm^3)	0.837×10^{-22}

3.9.2 Z-scan technique

Centrosymmetric crystal structures obeying TONLO properties (χ^3) were investigated by using Z-scan studies. To perform this study, a test sample (thickness 1 mm) was mounted on a sample container, and the laser power (25 mW) was focused on the focal length (20 cm) to generate a beam waist (ω_0) of 12.04 µm. The stepper moved from the + Z to − Z axis when the focussed Gaussian laser beam went through a crystal surface. The process of Z-scan transmittance was recorded using a detector connected to the digital power meter. The estimated Rayleigh length (Z_R) is 0.76 mm (Shettigar et al. 2007). The parameters non-linear refractive index (n_2) for open aperture (OA) and absorption coefficient (β) for closed aperture (CA) are displayed in Fig. 12a and b. As a result, the Z-scan pattern with strong non-linear absorption exhibits saturable absorption (SA), which happens when the excited state absorption cross-section exceeds that of the ground state. Whereas CA shows that the peak-to-valley signature indicating self-defocusing (SDF) nature of the material due to the negative refractive index nonlinearity. The calculated linear aperture transmittance (S) value is 0.52. On-axis phase shift (ΔΦ) value is 0.28. The standard relations of refractive index (n_2) and absorption (β) are experimentally calculated by using the formula (Sheik-Bahae 1990)

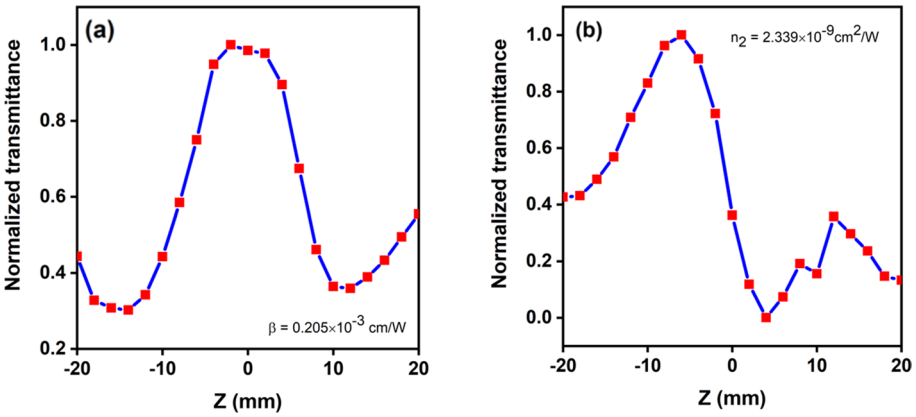

Fig. 12 **a** Open **b** Closed aperture Z-scan patterns

$$n_2 = \frac{\Delta\Phi}{KI_0L_{eff}}\left(\frac{\mathrm{m}^2}{\mathrm{w}}\right) \tag{13}$$

$$\beta = \frac{2\sqrt{2}\ \Delta\mathrm{T}}{I_0L_{eff}}\left(\frac{\mathrm{m}}{\mathrm{w}}\right) \tag{14}$$

where, wave vector ($K=2\pi/\lambda$), I_o represent laser beam intensity, ΔT is transmittance difference in OA and L_{eff} is effective sample thickness. Real and Imaginary parts of χ^3 relations (Desalvo 1993)

$$R_e(\chi^3)esu = \frac{10^{-4}\varepsilon_0C^2n_0^2n_2}{\pi}\left(\frac{\mathrm{cm}^2}{\mathrm{w}}\right) \tag{15}$$

$$I_m(\chi^3)esu = \frac{10^{-2}\varepsilon_0C^2n_0^2\lambda\beta}{4\pi^2}\left(\frac{\mathrm{cm}}{\mathrm{w}}\right) \tag{16}$$

The third order (χ^3) susceptibility and second-order hyper polarizability (γ) estimated by the relations (Stryland et al. 1998; Subashini et al. 2011)

$$\chi^3 = \sqrt{\left(\mathrm{R}_e(\chi^3)\right)^2 + \left(\mathrm{I}_m(\chi^3)\right)^2} \tag{17}$$

$$\gamma = \frac{\chi^{(3)}}{N^*f^4} \tag{18}$$

The coupling factor (ρ^*)

$$\rho^* = \frac{I_m(\chi^3)}{\mathrm{R}_e(\chi^3)} \tag{19}$$

The experimentally calculated TONLO properties are $n_2 = 2.33\times10^{-9}$ cm^2 W^{-1} and $\beta = 0.20\times10^{-3}$ cm W^{-1}. The χ^3 and γ were determined to be 1.49×10^{-5} esu (2.08×10^{-13} (m^2/v^2)) and 6.35×10^{-27} esu, respectively. The organometallic thiocyanate family crystals of MCCTC (Ramesh et al. 2019) compared to BDBCZTC nearly matched the value of TONLO presented in Table 9. Hence addressing the IPOS complex with a TONLO crystal (BDBCZTC) makes them a promising candidate for optical switching applications.

4 Conclusion

A novel BDBCZTC single crystal were grown by using the slow evaporation method. SXRD data shows that monoclinic system has space group $P2_1/n$. The estimated lattice dimensions are well-matched in both PXRD and SXRD. The existence of CN stretching of SCN, metal-nitrogen bonding and Ba–O group were confirmed by FT-IR and micro-Raman studies. The UV cut-off wavelength was found at 276 nm and band gap value is 4.1 eV. The FE-SEM micrograph clearly reveals the well-ordered small

Table 9 Comparison for TONLO properties of BDBCZTC crystal to other thiocyanate MCCTC crystal

Z-Scan parameters	BDBCZTC	MCCTC
Laser type	He–Ne laser	He–Ne laser
Wavelength of laser (nm)	633	633
Focal length (f) cm	20	–
Laser beam-diameter (cm)	0.1	–
Sample thickness (cm)	0.1	–
Aperture radius (mm)	3.3	–
Intensity of the laser (KW/cm^2)	1.784	–
Optical path distance (mm)	1	–
Beam waist (ω_0) μm	12.04	–
Rayleigh length (Z_R) mm	0.76	–
Effective thickness (L_{eff}) mm	0.49	
Refractive index n_2 (cm^2/W)	2.33×10^{-9}	8.57×10^{-13}
Absorption coefficient β (cm/W)	0.20×10^{-3}	8.14×10^{-6}
Real part of TONLO [R_e (χ^3)] (cm^2/W)	10.39×10^{-6}	–
Imaginary part of TONLO [I_m (χ^3)] (cm/W)	4.59×10^{-6}	–
TONLO (χ^3) esu	1.49×10^{-5} (2.08×10^{-13} (m^2/v^2))	2.49×10^{-9}
Second order molecular hyper polarizability (γ) esu	6.35×10^{-27}	–
Number of molecules per cm^3 (N*)	$9.64\times10^{+20}$	–
Coupling factor (ρ*)	2.261	–

micro-crystal-like morphological patterns are evident which shows the perfect growth of the 2D nucleation mechanism. The presence of elements (C_{32} H_{40} Ba Zn N_4 O_{10} S_4) were identified by using an EDS and CHNS analyser. The sample decomposition temperature is 334 °C compared to other IPOS complex crystals such as MCCTC (171 °C), and CMTD (150 °C). The mechanical strength of the grown crystal belongs to the hard materials category ($n = 1.19$). The dielectric constant and dielectric loss were varied by varying the frequency with temperature. Furthermore, SSP are theoretically calculated. From the Z-scan pattern, assess SA and SDF nonlinearity. The calculated values of refractive index ($n_2 = 2.33\times10^{-9}$ cm^{2}W^{-1}), absorption coefficient ($\beta = 0.20\times10^{-3}$ cmW^{-1}) and TONLO ($\chi^3 = 1.49\times10^{-5}$ esu), respectively. Therefore, the title compound has moderate mechanical, thermal stability and TONLO properties, which is suitable for optical limiting and optical switching applications.

Acknowledgements The authors are grateful thanks to SRM Institute of science and technology (Deemed University), Kattankulathur, Chengalpattu Dist, Tamilnadu, India provided major instrumentation speciality SRM-NRC, and micro-Raman SRM-SCIF.

Author contributions All authors contributed equally. All authors read and approved the final manuscript.

Funding The authors declare that no funds, grands, or other support were receive during the preparation of this manuscript.

Data Availability The data that support the findings of this study are available from the corresponding author upon reasonable request.

Declarations

Conflict of interest The authors declare that they have no conflict of interest. The authors have no relevant financial or non-financial interests to disclose.

References

Balarew, C., Duhlew, R.: Application of the hard and soft acids and bases concept to explain ligand coordination in double structures. J. Solid State Chem. **55**, 1–6 (1984)

Bruker AXS. Bruker AXS Inc. Madison (2008)

Cynthia, S., Milton Boaz, B.: Synthesis growth and characterization of a novel nonlinear optical crystal: CMTD. J. Appl. Phy. **3**, 6–11 (2013)

Cynthia, S., Sagadevan, S., Mariappan, L.: Investigation on the linear, non-linear and optical studies of an efficient organometallic zinc cadmium thiocyanate nonlinear optical complex crystal. J. Mater. Sci: Mater. Electron. **28**, 14787–14797 (2017)

Desalvo, R., Sheik-Bahae, M., Said, A., Hagan, D.J., Van Stryland, E.W.: Z-scan measurements of the anisotropy of nonlinear refraction and absorption in crystals. Opt. Lett. **18**, 194–196 (1993)

Gunasekaran, S., Ponnusamy, S.: Growth and characterization of cadmium magnesium tetra thiocyanate crystals. Cryst. Res. Technol. **41**, 130–137 (2006)

Hegde, T.A., Dutta, A., Gandhiraj, V.: $\chi 3$ measurement and optical limiting behavior of novel semi-organic cadmium mercury thiocynate crystal by Z-scan technique: CMTC. Appl. Phy. A **124**, 80 (2018)

Hegde, T.A., Dutta, A., Gandhiraj, V.: Review on growth and characterization of nonlinear optical organometallic thiocyanate crystals. Int. J. Eng. Technol. Innov. **9**(4), 257–289 (2019)

Jackson, J.D.: Classical electrodynamics. Wiley Eastern Limited, USA (1978)

Joseph, G.P., Philip, J., Rajarajan, K., Rajasekar, S.A., Pragasam, A.J., Thamizharasan, K., Kumar, S.R., Sagayaraj, P.: Growth and characterization of an organometallic nonlinear optical crystal of MMTC. J. Crystal Growth **296**, 51–57 (2006)

Kumar, L.B., Murthy, K.K., Rajeev, Y.N., Madhavan, J., Sagayaraj, P., Cole, S.: Influence of rare earth doping on the spectral, thermal, morphological and optical properties of nonlinear optical single crystal of manganese mercury thiocyanate $MnHg(SCN)_4$. Optik **126**, 4899 (2015)

Kumar, K.S., Baskaran, A., Ramesh, V., Murugavel, S., Sagayaraj, P., Rajarajan, K.: Synthesis growth spectral, optical and thermal properties of a novel metal-organic family single crystal: Bis (thiocyanate) Cobalt II di thiourea. Optick-Int. J. Light Electron Opt. **127**, 4964–5496 (2016)

Nijboer, B.R.A., Renne, M.J.: Microscopic derivation of macroscopic Vander waals forces. Chem. Phys. Lett. **2**, 35 (1968)

Pabitha, G., Dhanasekaran, R.: Investigation on the crystal growth and characterization of an organometallic nonlinear optical crystal Tetrathiourea mercury tetrathiocynate manganite. Mater. Sci. Eng., B **177**, 1149–1155 (2012)

Penn, D.R.: Wave number dependent dielectrics function of semiconductors. Phys. Rev. **128**, 2093–2097 (1962)

Rajarajan, K., Sendil Kumar, K.: Spectroscopic, optical, thermal, and AC conductivity studies on semi-organic nonlinear optical crystal: AMCTC. J. Therm Anal. Calorium **112**, 1297–1302 (2013)

Ramesh, V., Rajarajan, K.: Crystal growth and characterization of a novel inorganic-organic hybrid NLO crystal: (NH_4) [Cd $(NCS)_3$].$C_{12}H_{24}O_6$]. Appl. Phys. B **113**, 99 (2013)

Ramesh, V., Gunasekaran, B., Krishnamohan, M., Rajarajan, K.: Synthesis, growth, linear and nonlinear optical, electrical and surface studies of a hybrid nonlinear optical material. Mater. Res. Express **6**, 116205 (2019)

Ramesh, V., Gunasekaran, B., Suresh, P., Sundaravadivel, E., Showrilu, K., Rajarajan, K.: Crystal growth, surface morphology, mechanical and thermal properties of UV-nonlinear optical crystal: mercury cadmium chloride thiocyanate (MCCTC) single crystal. Mater. Sci. Eng. **872**, 012175 (2020)

Ravindra, N.M., Srivastava, V.K.: Electronic polarizability as a function of the penn gap in semiconductors. J. Infrared Phys. **20**, 67–69 (1980)

Ravisankar, V., Ramesh, V., Gunasekaran, B., Krishnamohan, M., Girisun, T.S., Dhanusha, A.: Synthesis, growth, structural and physicochemical properties of a novel linear and nonlinear uv-optical single-crystal for photonic applications: [Ba $(C1_4H_{20}O_5)$2.Co $(SCN)_4$]. ECS J. Solid State Sci. Tech. **10**, 09100 (2021a)

Ravisankar, V., Ramesh, V., Sridevi, V., Gunasekarana, B.: Synthesis, growth, structural, physicochemical, linear and nonlinear optical properties of new hybrid [(Ba(C10H20O5)2)· (Mn $(SCN)_4$)] single crystal. Appl. Phys. A **127**, 885 (2021b)

Ravisankar, V., Ramesh, V., Krishnamohan, M., Gunasekarana, B., Sabari Girisun, T.S.: Bis(benzo-15-crown-5-j5 O)barium tetraki (isothiocyanatokN)cobaltate(II). IUCrData **6**, 2414–3146 (2021c)

Ravisankar, V., Ramesh, V., Gunasekaran, B., Girisun, T.S.: Synthesis, growth, structural, physicochemical, linear, and nonlinear optical properties of new hybrid [2(C10H20O5) Ba] [Co $(SCN)_4$] single crystal. J. Mater. Sci: Mater. Electron. **33**, 9380–9394 (2022)

Sakthi, P., Rajasekaran, R., Balasubramanian, D.: Growth, optical, thermal and mechanical behavior of an organometallic nonlinear optical –thiocyanate thiourea potassium chloride single crystal. J. Adv. Phys. **5**, 199–206 (2016)

Saravanan, N., Chidambaram, V., Ravisankar, V.: Growth and characterization of novel semi organic nonlinear optical urea lead acetate single crystal by solution growth technique. J. Mater. Sci: Mater. Electron. **29**, 5009–5013 (2018)

Sheik-Bahae, M.: Sensitive measurement of optical nonlinearities using a single beam. J. Quantum. Electron. **26**, 760–769 (1990)

Sheldrick, G.M.: SADABS program for area detector absorption. Correction Institute for Inorganic Chemistry. University of Gottingen, Germany (1996)

Sheldrick, G.M.: A short history of SHELX. Acta Cryst. **A64**, 112–122 (2008)

Shettigar, S., Umesh, G., Chandrasekharan, K., Kalluraya, B.: Third-order nonlinear optical properties and two-photon absorption in newly synthesized phenylsydnone doped polymer. Synth. Met. **157**(15), 142–146 (2007)

Showrilu, K., Ramesh, V., Rajarajan, K., Dhas, S.M.: Synthesis, growth, structure, spectroscopic, and physicochemical properties of 18-Crown-6-ether barium (II) bisthiocyanate monohydrate single crystal: BCBT. Mater. Sci. Engg. **872**, 012136 (2020)

Subashini, A., Kumaravel, R., Leela, S., Evans, H.S., Sastikumar, D., Ramamurthi, K.: Synthesis, growth and characterization of 4-bromo-4'chloro benzylidene aniline-a third order nonlinear optical material. Spe. Chimica Acta a, Mol Biomole Spe **78**, 935–941 (2011)

Sun, H.Q., Yuan, D.R., Wang, X.Q., Cheng, X.F., Gong, C.R., Zhou, M., Xu, H.Y., Wei, X.C., Luan, C.N., Pan, D.Y., Li, Z.F.: A novel metal-organic coordination complex crystal: tri-allylthiourea Zinc chloride. Cryst. Res. Technol. **40**, 882–886 (2005)

Sundararaj, C., Sagadevan, S.: Synthesis and characterization of non-linear optical crystal of manganese mercury thiocyanate glycol monomethyl ether. Mater. Res. (2018). https://doi.org/10.1590/1980-5373-MR-2016-0595

Suresh, T., Vetrivel, S., Gopinath, S., Vinoth, E.: A new NLO material L-Asparagine thiocynate for opto electronic applications: LATC. Chi. J. Phy. **18**, 9 (2018)

Usha, R.J., Suganthi, A.B., Sagayara, P., Joseph, V.: Mechanical and optical analyses of cadmium mercury thiocynate single crystal. Spectrosc. Lett. **48**, 74–77 (2015)

Van Stryland, E.W., Sheik-Bahae, M., Kuzyk, M.G., Dirk, C.W.: Z-scan measurements of characterization techniques and tabulations for organic nonlinear materials. Charact. Techn. Tabul Org. Nonlinear Mater. **18**, 655–692 (1998)

VethaPotheher, I., Rajarajan, K., Jeyasekaran, R., Vimalan, M., Yogam, F., Sagayaraj, P.: Growth, optical, thermal, and conductivity behavior of nonlinear optical single crystals of CMTG. J. Therm. Anal Calorim **111**, 1491–1497 (2013)

Vijayabhaskaran, B., Raja, C.R.: Influence of metallic substitution on the physical properties of nickel mercury thiocyanate nonlinear optical crystal. Optick **124**, 1366–1368 (2013)

Authors and Affiliations

V. Ravisankar[1] · V. Ramesh[1] · B. Gunasekaran[1] · Suresh Perumal[2] · P. Karuppasasmy[3] · T. Kamalesh[4]

✉ B. Gunasekaran
gunasekb@srmist.edu.in; phdguna@gmail.com

V. Ravisankar
vrss87@gmail.com

V. Ramesh
rameshmano1980@gmail.com

Suresh Perumal
drsureshperumal@gmail.com

P. Karuppasasmy
karuppasamyp@ssn.edu.in

T. Kamalesh
kamaleshkamal918@gmail.com

[1] Department of Physics and Nanotechnology, SRM Institute of Science and Technology, Kattankulathur, Chennai, Tamil Nadu 603203, India

[2] Department of Materials Science and Metallurgical Engineering, IIT, Hyderabad, Telangana 502285, India

[3] Crystal Growth Research Center, SSN College of Engineering, Chennai, Tamil Nadu 603110, India

[4] Department of Physics, B. S. Abdur Rahman Crescent Institute of Science and Technology, Chennai, Tamil Nadu 600048, India